

Reliable Grid Forecasting: State Space Models for Safety-Critical Energy Systems

Jisoo Lee and Sunki Hong

Gramm AI.

*Corresponding author(s). E-mail(s): jisoo@gramm.ai;
Contributing authors: sunki@gramm.ai;

Abstract

Accurate grid load forecasting is safety-critical: under-predictions risk supply shortfalls, while symmetric error metrics mask this operational asymmetry. We introduce a grid-specific evaluation framework—Asymmetric MAPE, Under-Prediction Rate, and Reserve Margin—that directly measures operational risk rather than statistical accuracy alone.

Using this framework, we conduct a systematic evaluation of Mamba-based State Space Models for California grid forecasting on a weather-aligned CA ISO-TAC dataset spanning Nov 2023–Nov 2025 (84,498 hourly records across 5 transmission areas). Our analysis reveals that standard accuracy metrics are poor proxies for operational safety: models with identical MAPE can require vastly different reserve margins.

We demonstrate that forecast errors are weakly but statistically significantly associated with temperature ($r = \mathbf{0.16}$), motivating weather-aware modeling rather than loss function modification alone. The S-Mamba model achieves the lowest Reserve_{99.5}[%] margin (14.12%) compared to 16.66% for iTransformer, demonstrating superior forecast reliability under a 99.5th-percentile tail-risk reserve proxy.

Keywords: Load forecasting, state space models, Mamba, deep learning, probabilistic forecasting, California grid, CAISO

1 Introduction

Short-term load forecasting (STLF) underpins electricity grid operations, governing unit commitment, economic dispatch, and reserve scheduling [1]. The consequences

are significant: under-prediction risks cascading blackouts, while over-prediction incurs unnecessary costs and emissions.

California’s grid exemplifies the challenges facing high-renewable systems. Solar and wind now account for 25% of generation [2], with behind-the-meter (BTM) solar contributing an additional 10–15% of midday native load. This invisible generation creates the “duck curve”—deep midday net load trough followed by steep evening ramps—that evolves annually as BTM capacity expands. Compounding this non-stationarity, climate-driven extreme weather events increasingly trigger non-linear demand spikes that defy historical patterns [3].

Existing forecasting methods face fundamental limitations. Statistical approaches (ARIMA) cannot capture non-linear weather dependencies [4]. Recurrent networks (LSTMs) struggle with long-range dependencies due to vanishing gradients. Transformer architectures address this but introduce quadratic $O(n^2)$ complexity, limiting practical context lengths for capturing multi-week seasonal patterns [5].

State space models (SSMs) offer a compelling path to reliability. By achieving linear $O(n)$ scaling, Mamba [6] allows for extended historical contexts and lower inference latency, freeing computational budget for robust uncertainty quantification and ensemble methods. However, Mamba’s ability to maintain safety margins in regional grid forecasting—characterized by asymmetric error costs and heteroscedasticity—remains unexplored.

We present a systematic evaluation of Mamba architectures for reliable California grid load forecasting. We benchmark against iTransformer and the foundation model Chronos, but shift the evaluation focus from pure accuracy to *operational safety*. Our analysis reveals that standard training objectives fail to capture the risk profile needed by operators; S-Mamba achieves a Reserve_{99.5} margin of 14.12%, significantly lower than the 16.66% required by iTransformer. Furthermore, we demonstrate that explicit weather integration is critical for safety, reducing the frequency of extreme (>1000 MW) error events by 40%.

Contributions

To move beyond symmetric accuracy metrics toward operator-relevant reliability for California grid forecasting, we make the following contributions:

1. **Grid-Specific Evaluation Framework.** We formalize operational risk metrics (α -MAPE, Under-Prediction Rate, Reserve Margin) that capture the asymmetric costs of forecast errors, demonstrating that standard metrics are poor proxies for grid safety (Section 2.3).
2. **Weather Integration for SSMs.** We develop and systematically evaluate thermal-lag-aligned weather fusion strategies for Mamba architectures, achieving 40% reduction in extreme errors (Section 6.5).
3. **Loss vs. Safety Analysis.** We show that loss reweighting alone cannot substitute for covariate modeling: quantile loss reduces >1000 MW errors by only 1.6% on CA ISO-TAC test windows, while weather-aware modeling yields materially larger tail-risk improvements (Section 6).

2 Background

2.1 State Space Models

State space models (SSMs) provide a principled framework for modeling sequential data through continuous-time dynamical systems. The general linear SSM is defined by the following ordinary differential equations:

$$h'(t) = Ah(t) + Bx(t), \quad y(t) = Ch(t) + Dx(t) \quad (1)$$

where $x(t) \in \mathbb{R}$ is the input signal, $h(t) \in \mathbb{R}^N$ is the latent state with dimension N , and $y(t) \in \mathbb{R}$ is the output. The matrices $A \in \mathbb{R}^{N \times N}$, $B \in \mathbb{R}^{N \times 1}$, $C \in \mathbb{R}^{1 \times N}$, and $D \in \mathbb{R}$ are learnable parameters.

For discrete-time computation on sampled data, the continuous SSM must be discretized. Using zero-order hold discretization with time step Δ , the discrete-time SSM becomes:

$$h_k = \bar{A}h_{k-1} + \bar{B}x_k, \quad y_k = Ch_k \quad (2)$$

where $\bar{A} = \exp(\Delta A)$ and $\bar{B} = (\Delta A)^{-1}(\exp(\Delta A) - I) \cdot \Delta B$.

Selective state spaces. Traditional SSMs employ time-invariant (LTI) parameters. The Mamba architecture [6] introduces a selective mechanism that makes these parameters input-dependent:

$$B_k = s_B(x_k), \quad C_k = s_C(x_k), \quad \Delta_k = \text{softplus}(s_\Delta(x_k)) \quad (3)$$

where s_B , s_C , and s_Δ are learned projections. This selectivity enables the model to filter relevant information while forgetting irrelevant context, addressing a fundamental limitation of prior SSMs.

Suitability for grid data. Recent analysis by Wang et al. [7] identifies conditions where Mamba outperforms Transformers: datasets with “numerous variates, most of which are periodic.” Grid load data matches this characterization precisely—highly periodic signals (daily/weekly cycles) across multiple spatial nodes. Mamba’s selective state mechanism encodes these rhythmic dependencies while filtering stochastic noise.

Computational complexity. SSMs achieve $O(n)$ complexity versus $O(n^2)$ for self-attention. Menati et al. [8] demonstrate that context windows of 240+ hours are optimal for capturing multi-scale grid dynamics—a length computationally prohibitive for standard Transformers.

2.2 Load Forecasting Fundamentals

Definition and Horizons. Short-term load forecasting (STLF) encompasses prediction of electricity demand from hours to days ahead [9]. Different forecast horizons serve distinct operational purposes: 1-hour for real-time dispatch, 4–6 hours for unit commitment, and 12–24 hours for day-ahead market operations.

Multi-Periodicity. Electricity load exhibits strong multi-periodic patterns (daily, weekly, annual). Our choice of 240-hour (10-day) context length ensures capture of at least one complete weekly cycle.

Evaluation Metrics. For load forecasting with positive data, mean absolute percentage error (MAPE) is the standard metric:

$$\text{MAPE} = \frac{100}{n} \sum_{i=1}^n \left| \frac{y_i - \hat{y}_i}{y_i} \right| \quad (4)$$

2.3 Grid-Specific Evaluation Metrics

Standard metrics like MAPE and RMSE treat forecast errors symmetrically: an over-prediction of 100 MW is penalized identically to an under-prediction of 100 MW. For grid utility operators, however, the economic and reliability consequences of these errors are fundamentally asymmetric [10].

2.3.1 The Asymmetry of Grid Operations

- **Over-Prediction (False Positive):** If the model predicts higher load than the actual demand, the utility commits excess generation. This results in financial loss (wasted fuel, curtailment costs) but rarely threatens system stability.
- **Under-Prediction (False Negative):** If the model predicts lower load than the actual demand, the utility may face a supply shortfall. This necessitates deploying expensive fast-ramping reserves (e.g., peaker plants), purchasing emergency power at spot market caps (often \$1,000+/MWh), or in extreme cases, initiating rolling blackouts.

Standard MAPE is therefore insufficient for operational validation. To address this, we introduce a suite of grid-specific metrics:

2.3.2 Proposed Metrics

Asymmetric MAPE (α -MAPE). We define a weighted MAPE that applies a penalty factor $\alpha > 1$ to under-predictions:

$$\alpha\text{-MAPE} = \frac{100}{n} \sum_{i=1}^n w_i \left| \frac{y_i - \hat{y}_i}{y_i} \right|, \quad w_i = \begin{cases} \alpha & \text{if } y_i > \hat{y}_i \\ 1 & \text{otherwise} \end{cases} \quad (5)$$

In this work, we use $\alpha = 2$, reflecting the industry consensus that under-prediction risks are approximately double the cost of over-prediction for day-ahead planning.

Under-Prediction Rate (UPR). The frequency of under-estimation events represents the probability of needing real-time upward dispatch:

$$\text{UPR} = \frac{1}{n} \sum_{i=1}^n \mathbb{I}(y_i > \hat{y}_i) \times 100\% \quad (6)$$

A naive model might achieve low MAPE by constantly under-predicting (taking the median); UPR exposes this risky behavior.

Reserve Margin Required. The additional upward capacity required to cover 99.5% of the *under-forecast* error distribution. We use the 99.5th percentile as a practical tail-risk proxy (motivated by resource adequacy practice; e.g., [11]). We report this both in megawatts (MW) and as a percentage of the point forecast (scale-free):

$$\text{Reserve}_{99.5}^{MW} = \text{Percentile}_{99.5}(\max(0, y - \hat{y})) \quad (7)$$

$$\text{Reserve}_{99.5}^{\%} = 100 \times \text{Percentile}_{99.5} \left(\max \left(0, \frac{y - \hat{y}}{\hat{y}} \right) \right) \quad (8)$$

Adding $\text{Reserve}_{99.5}^{MW}$ to the point forecast covers 99.5% of historical under-prediction events at the evaluated horizon. We report both MW and percentage: MW is normalization-free, while the percentage form is directly interpretable as an *add-on* to the scheduled point forecast. Because percentage-normalized reserve can be biased by systematic forecast inflation, we always interpret $\text{Reserve}_{99.5}^{\%}$ jointly with α -MAPE and UPR to ensure improvements do not come from trivial over-forecasting.

2.3.3 Why Metrics Matter: A Real-World Case Study

To illustrate the operational reality of these metrics, we compare two architectures from our experimental results (Table 2) applied to a hypothetical 25,000 MW California grid system.

PowerMamba: Achieves better average accuracy (4.37% MAPE) but a high Under-Prediction Rate (58.8%) and Reserve Requirement (21.68%).

S-Mamba: Achieves slightly worse accuracy (4.77% MAPE) but significantly lower UPR (40.9%) and Reserve Requirement (14.12%).

Operational Implication.

Although PowerMamba appears superior by only looking at MAPE, its error structure is operationally expensive. The $\text{Reserve}_{99.5}^{\%}$ difference ($21.68\% - 14.12\% = 7.56\%$) implies that, for a representative 25,000 MW day-ahead point forecast, an operator using PowerMamba must schedule an additional 1,890 MW of spinning reserves every hour ($25,000 \text{ MW} \times 7.56\%$).

Assuming a typical reserve holding cost of \$10/MW-h, deploying the “more accurate” PowerMamba model would incur approximately \$453,600 per day in excess ancillary service costs compared to S-Mamba. This paradox—where the model with better MAPE costs more to operate—demonstrates why our evaluation prioritizes α -MAPE, UPR, and Reserve metrics alongside standard accuracy.

2.3.4 From Metrics to Optimization

While α -MAPE and UPR are excellent for evaluation, they are non-differentiable and difficult to optimize directly. To bridge this gap, we employ **Quantile Loss** (Pinball Loss) as a differentiable surrogate during the training process (specifically Phase 3, see Section 5.5).

The quantile loss for a target quantile q is defined as:

$$\mathcal{L}_q(y, \hat{y}) = \max(q(y - \hat{y}), (1 - q)(\hat{y} - y)) \quad (9)$$

By training on high quantiles (e.g., $q = 0.9$), we effectively apply a higher gradient penalty to under-predictions (weighted by q) than over-predictions (weighted by $1 - q$). This aligns the model’s statistical objective with the operator’s economic objective, naturally suppressing the UPR and improving α -MAPE without requiring custom non-convex loss functions. We evaluate empirically whether this theoretical alignment translates to practice in Section 6.

2.4 CAISO Market Context and Benchmarks

The California Independent System Operator (CAISO) operates two primary energy markets demanding distinct forecast horizons: the Day-Ahead Market (DAM) requiring hourly forecasts submitted by 10:00 AM the prior day, and the Real-Time Market (RTM) requiring 5-minute granularity. A defining feature of the CAISO control area is the massive penetration of Behind-the-Meter (BTM) solar, which serves approximately 10–15% of native load during midday.

This BTM capacity physically disconnects “gross load” (total consumption) from “net load” (visible grid demand), creating the well-known “duck curve” phenomenon. This introduces a critical weather dependency: cloud cover variations cause instantaneous ramp events that statistical baselines struggle to predict.

Operational load forecasts serve as the industry benchmark. During the July 2024 heat wave (July 4–12), third-party analysis reported CAISO’s day-ahead forecast achieved 4.55% MAPE, while commercial forecasting services achieved 2.65% MAPE—a 41% improvement [12]. These benchmarks establish minimum performance targets for operational deployment.

Accurate forecasting during extreme weather events is critical. The July 2024 analysis revealed CAISO’s peak load forecast error of 3,211 MW during the heat wave, highlighting the importance of weather-integrated forecasting approaches.

3 Related Work

3.1 Deep Learning for Time Series

Deep learning has systematically displaced statistical methods (ARIMA, SVR) for short-term load forecasting due to its superior ability to model non-linear relationships. Current research focuses on two primary paradigms for long-context multivariate modeling:

Transformer-based Approaches. Computing global attention allows Transformers to capture long-range dependencies, but with $O(n^2)$ complexity. Two main strategies have emerged to handle multivariate data:

- *Channel Independence:* Models like **PatchTST** [13] treat multivariate time series as independent channels and segment them into patches. This reduces complexity and

represents the current state-of-the-art for Transformer accuracy, though it sacrifices explicit cross-variable correlation modeling.

- *Multivariate Attention*: Models like **iTransformer** [14] explicitly model correlations between variables by inverting tokenization (embedding time steps as features). We study iTransformer as a primary baseline because its explicit modeling of spatial correlations (e.g., between load and weather variables) offers a direct contrast to the implicit state mixing of Mamba.

Efficient Sequence Modeling (SSMs). State space models offer a fundamentally different approach. Instead of the quadratic global attention of Transformers, SSMs like Mamba [6] employ a recurrent mode with input-dependent selection, achieving linear $O(n)$ scaling. This efficiency allows for significantly longer context windows (240+ hours) on the same hardware, potentially capturing seasonal patterns that are computationally prohibitive for attention-based models.

Linear Models. Recent work has challenged the necessity of deep learning for time series forecasting. DLinear [15] demonstrates that simple linear models often match or exceed Transformer performance on standard benchmarks, raising questions about architectural complexity. However, linear models cannot capture non-linear temperature-load relationships that dominate during extreme weather events—precisely when forecast accuracy is most critical for grid operations. Our evaluation focuses on models capable of learning these non-linear interactions.

This work systematically evaluates whether the theoretical efficiency advantage of Mamba translates to superior accuracy on complex, real-world grid data compared to the expressive power of multivariate Transformers.

3.2 State Space Models for Time Series

The Structured State Space (S4) model [16] introduced efficient long-range sequence modeling through careful parameterization of continuous-time state spaces. Mamba [6] extended this framework with input-dependent (selective) parameters, enabling content-aware filtering that improves performance on language and genomics tasks. For time series specifically, S-Mamba [7] demonstrated that Mamba architectures excel on datasets with “numerous variates, most of which are periodic”—a characterization that matches grid load data. PowerMamba [8] introduced bidirectional processing and series decomposition specifically for energy applications, showing that 240+ hour context windows are optimal for capturing multi-scale grid dynamics.

3.3 Weather-Integrated Forecasting

The relationship between weather and electricity demand is well-established [10]. Temperature-based load models form the basis of many operational forecasting systems, with heating and cooling degree days serving as primary predictors. However, integrating weather into deep learning architectures remains challenging due to temporal misalignment: building thermal mass introduces response lags of 2–6 hours between temperature changes and load response [17]. Prior work has addressed this through feature engineering [18] or attention mechanisms [9], but systematic evaluation of weather integration strategies for state space models is lacking.

3.4 Foundation Models for Time Series

Pre-trained foundation models have recently emerged as alternatives to task-specific architectures. Chronos [19] adapts language model pre-training to time series through quantization, demonstrating strong zero-shot performance on diverse forecasting benchmarks. However, the effectiveness of foundation models on domain-specific tasks with strong exogenous dependencies (e.g., weather-driven load) remains an open question, as these models typically lack mechanisms for incorporating auxiliary covariates.

4 Methodology

4.1 Model Architectures

We evaluate three Mamba-based architectures representing different design philosophies within the state space model paradigm, alongside the iTransformer baseline.

4.1.1 S-Mamba: The Linear-Time Baseline

S-Mamba [7] represents a minimalist approach to state space modeling. It adapts the standard Mamba block for time series via a simple encoder-decoder structure: a linear projection embeds the input sequence into a hidden state D , followed by stacked Mamba layers.

The primary goal of S-Mamba is to test whether the core selective state space mechanism alone—without complex decomposition or attention—is sufficient to model grid dynamics. Its design prioritizes computational efficiency ($O(n)$ complexity) above all else, making it an ideal candidate for resource-constrained edge deployment (0.08ms inference latency).

4.1.2 PowerMamba: Physics-Aware Decomposition

PowerMamba [8] addresses a specific limitation of standard SSMS: the difficulty of modeling disparate frequencies (e.g., long-term trend vs. daily seasonality) within a single state vector.

PowerMamba introduces two critical innovations for energy data:

- *Series Decomposition*: It splits the input into "Trend" (low-frequency) and "Seasonal" (high-frequency) components, and processes them via independent Mamba encoders. This explicitly separates the "duck curve" drift from daily load cycles.
- *Bidirectionality*: Unlike language modeling where causality is strict (future cannot affect past), time series analysis benefits from looking forward (e.g., smoothing). PowerMamba processes sequences in both forward and backward directions to capture a holistic temporal context.

4.1.3 Mamba-ProbTSF: From Point Signals to Risk Management

Grid operators rarely make decisions based on a single deterministic number; they require confidence intervals to schedule reserves. Mamba-ProbTSF extends the architecture with a probabilistic output head.

The varying nature of renewable generation introduces heteroscedastic noise—uncertainty that changes over time (e.g., higher uncertainty at sunset). Mamba-ProbTSP replaces the standard linear readout with a Gaussian head that predicts both mean μ and variance σ^2 :

$$\mathcal{L} = \frac{1}{2} \left[\log(\sigma^2) + \frac{(y - \mu)^2}{\sigma^2} \right] \quad (10)$$

This shift from minimizing MSE to maximizing likelihood enables the model to quantify “known unknowns,” providing actionable risk metrics for uncertainty-aware dispatch.

4.1.4 iTransformer: The Strongest Multivariate Baseline

The iTransformer [14] challenges the standard Transformer paradigm. Instead of tokenizing time steps (embedding T steps into vectors), it tokenizes *variables* (embedding the entire time series of a variate as a single token).

Standard Transformers struggle to model correlations between different sensors (or grid nodes) because they treat them as channels within a time-step token. iTransformer inverts this: the self-attention mechanism computes correlations *between variables* (e.g., Load vs. Temperature), explicitly modeling the system-wide interdependencies critical for grid stability. We include this baseline to rigorously test whether Mamba’s implicit state mixing can compete with iTransformer’s explicit correlation modeling.

5 Experimental Setup

5.1 Dataset

We use hourly load data from CAISO (Nov 2023–Nov 2025), comprising 84,498 hourly records across 5 major transmission access charge (TAC) areas: CA ISO-TAC (system aggregate), PGE-TAC, SCE-TAC, SDGE-TAC, and TIDC. Following PowerMamba [8], we adopt a 240-hour (10-day) context window to capture at least one complete weekly cycle, enabling models to learn both daily and weekly periodicity patterns.

Preprocessing. Load values are normalized using z-score standardization computed only on training data to prevent information leakage. Temporal features include hour-of-day (0–23) and day-of-week (0–6), encoded as sinusoidal embeddings following standard practice [20]. For weather-integrated models, we include 8 meteorological covariates with thermal lag alignment, as described in Section 5.2.

5.2 Thermal Lag Analysis and Justification

A critical design decision for weather-integrated forecasting is the temporal alignment between meteorological variables and load response. Buildings do not respond instantaneously to temperature changes; rather, the thermal mass of walls, floors, and furnishings creates a delayed response in HVAC demand. We conducted a systematic cross-correlation analysis to determine optimal lag values empirically.

Cross-Correlation Methodology. For each weather covariate w_t and the load signal L_t , we computed the Pearson correlation coefficient at lag $\tau \in \{0, 1, 2, \dots, 12\}$ hours:

$$\rho(\tau) = \text{Corr}(w_{t-\tau}, L_t) \quad (11)$$

The optimal lag $\tau^* = \arg \max_{\tau} |\rho(\tau)|$.

Empirical Results. Analysis of the Nov 2023–Nov 2025 hourly dataset (84,498 records across 5 TAC areas) reveals distinct lag patterns by covariate type:

- **Temperature (dry bulb):** Peak correlation at $\tau = 3$ hours ($\rho = 0.72$), consistent with commercial building thermal time constants of 2–4 hours reported in building physics literature [17]. Residential buildings show shorter lags (1–2 hours) while large commercial buildings exhibit lags up to 6 hours.
- **Solar radiation (GHI):** Peak correlation at $\tau = 1$ hour ($\rho = 0.45$), reflecting the more immediate effect of solar heat gain through windows and the subsequent building envelope heating.
- **Humidity:** Peak correlation at $\tau = 3$ hours ($\rho = 0.38$), as latent cooling loads follow similar thermal dynamics to sensible loads.
- **Wind speed:** Minimal lag ($\tau = 0$ –1 hour, $\rho = 0.12$), as ventilation effects manifest more quickly.

Physical Interpretation. The observed 2–6 hour lag range aligns with building thermal dynamics theory. Seem [17] models commercial building response using first-order thermal networks with time constants $\tau_{building} = RC$, where R is thermal resistance and C is thermal capacitance. For typical California commercial buildings:

- Light construction (steel frame, single-pane): $\tau \approx 1$ –2 hours
- Medium construction (concrete tilt-up): $\tau \approx 3$ –4 hours
- Heavy construction (concrete/masonry): $\tau \approx 5$ –6 hours

The aggregate California load reflects a mixture of building types, with commercial buildings dominating peak demand. Our empirically-derived lags of 2–4 hours for temperature-related covariates are consistent with this physical understanding.

Horizon-Adaptive Alignment. For multi-horizon forecasting, we apply horizon-adaptive lag adjustment. When forecasting load at time $t+h$ for horizon h , the effective lag becomes $\tau_{eff} = \tau^* + h$. Weather features at time t are aligned to predict load response at $t + \tau^* + h$, ensuring consistent temporal relationships across all forecast horizons.

Train/Validation/Test Split. We employ chronological splitting to respect temporal dependencies: 70% training, 15% validation, and 15% test within each TAC-area time series. Due to minor missingness differences by region, exact split dates vary slightly by utility; for CA ISO-TAC, the split is train (2023-11-01–2025-04-09), validation (2025-04-09–2025-07-31), and test (2025-07-31–2025-11-22). This non-overlapping split ensures evaluation on future, unseen data—critical for operational deployment assessment. For evaluation, we construct sliding windows with 240-hour context and 48-hour prediction horizon; for CA ISO-TAC, the 2,649-hour test segment yields 2,362 forecast windows.

5.3 Models Under Comparison

We evaluate three Mamba-based architectures against established baselines, enabling direct comparison across parameter efficiency and accuracy.

Proposed Mamba Architectures:

- **S-Mamba** (16.4M): Minimal SSM architecture with an MLP projection head, testing whether selective state spaces alone suffice for grid dynamics.
- **PowerMamba** (2.5M): Series decomposition with bidirectional processing and a lightweight projection head for multi-scale patterns.
- **Mamba-ProbT5F** (16.4M): Risk-aware variant sharing the S-Mamba backbone with an uncertainty-/risk-oriented output parameterization.

Baselines:

- **LSTM** [1]: 2-layer LSTM (0.21M parameters), representing the industry-standard recurrent approach.
- **iTransformer** [14]: Inverted Transformer baseline used in our experiments (50.0M parameters), representing a strong attention-based forecasting model.
- **Chronos-T5-Small** [19]: 8M-parameter foundation model evaluated in zero-shot regime.

This comparison directly tests whether Mamba’s $O(n)$ efficiency can match the accuracy of larger Transformer models. PowerMamba (2.5M parameters) is particularly compact, while S-Mamba and Mamba-ProbT5F (16.4M parameters) trade parameter count for expressive projection heads.

5.4 Model Hyperparameters

Following the experimental protocol of PowerMamba [8], all Mamba variants share consistent architectural hyperparameters: $d_{model} = 128$ (embedding dimension), $d_{state} = 16$ (state dimension), $d_{conv} = 4$ (convolution kernel), expansion factor 2, and 2 bidirectional encoder layers. Parameter counts differ due to projection head design: PowerMamba uses a linear head (2.5M total), while S-Mamba and Mamba-ProbT5F use MLP heads (16.4M total). Dropout rate is 0.1 across all models. Weather integration adds negligible parameters ($\sim 1K$ for the weather embedding layer).

5.5 Training Protocol

Optimization. We use AdamW optimizer with weight decay 10^{-5} . Learning rate follows cosine annealing from 3×10^{-5} to 10^{-7} over 300 epochs with 10-epoch linear warmup. Early stopping monitors validation MAPE with patience 30 to prevent overfitting. Batch size is 32 for Mamba variants, 512 for LSTM, and 4096 for iTransformer (adjusted for GPU memory).

Three-Phase Hybrid Training Strategy. We implement a training protocol designed for non-stationary grid data:

1. **Phase 1 (Pattern Extraction):** Pre-training on the full available history with MSE loss (50 epochs, lr= 10^{-3} , batch=1536). This phase learns stable seasonal and weekly patterns.
2. **Phase 2 (Drift Adaptation):** Fine-tuning on the most recent segment with MSE loss (20 epochs, lr= 10^{-4}). This phase adapts to recent “duck curve” evolution and BTM solar growth.
3. **Phase 3 (Tail Annealing):** Refinement with quantile loss at $q \in \{0.025, 0.5, 0.975\}$ with risk weights [4, 1, 4] to suppress extreme errors while maintaining central tendency.

Reproducibility. All experiments run on NVIDIA RTX 5090 GPUs. In this draft, we report results for a fixed random seed (42). Code and configurations are available for reproducibility.

5.6 Evaluation Metrics

Primary metric is MAPE evaluated at multiple horizons (1h, 6h, 12h, 24h). For tail error analysis, we report counts of errors exceeding operational thresholds (1000, 1500, 2000 MW).

5.7 Statistical Analysis

We report point-estimate metrics on the held-out test split. Statistical significance and multi-seed robustness analysis are left for future work.

6 Results

6.1 Multi-Horizon Performance

Table 1 presents the MAPE comparison. PowerMamba excels at the 1-hour horizon (2.40%) and the 24-hour horizon (4.13%). For day-ahead (24h) forecasts, all Mamba variants outperform the 50.0M parameter iTransformer and the foundation model Chronos on CA ISO-TAC.

Table 1: Multi-horizon accuracy comparison on CA ISO-TAC. MAPE (%) across forecast horizons for a fixed random seed (42). Weather-integrated variants are evaluated in Section 6.5; best results are in bold.

Model	Params	1h	6h	12h	24h
S-Mamba	16.4M	2.49	3.78	4.09	4.62
Mamba-ProbTSF	16.4M	2.28	3.43	3.70	4.29
PowerMamba	2.5M	2.40	3.62	4.03	4.13
LSTM	0.21M	5.41	5.59	5.64	6.49
iTransformer	50.0M	3.00	3.93	4.26	4.69
Chronos (zero-shot)	8.0M	2.50	3.68	4.84	5.23

Table 2: Grid safety metrics reveal risk not captured by MAPE. Results at 24h for risk-averse calibrated models: α -MAPE penalizes under-prediction ($\alpha = 2$), UPR is the under-prediction frequency, and $\text{Reserve}_{99.5}^{\%}$ is the 99.5th percentile one-sided under-forecast error as a fraction of the point forecast (Section 2.3).

Model	MAPE	α -MAPE	UPR	$\text{Reserve}_{99.5}^{\%}$
LSTM Baseline	6.62%	9.95%	50.8%	25.07%
iTransformer	4.93%	6.62%	40.7%	16.66%
Mamba-ProbTSF	4.14%	5.84%	44.4%	16.32%
PowerMamba	4.37%	7.16%	58.8%	21.68%
S-Mamba (Ours)	4.77%	6.31%	40.9%	14.12%

Notably, S-Mamba offers a superior risk-adjusted profile, reducing under-prediction risk ($\text{Reserve}_{99.5}^{\%}$: 25.07% \rightarrow 14.12%, a 43.7% reduction) compared to the LSTM baseline, while PowerMamba exhibits high UPR (58.8%) despite competitive MAPE.

6.2 Error Analysis: The Loss Function Hypothesis

While baseline Mamba models achieve strong average performance (Table 1), analysis of the error distribution reveals persistent large errors that pose operational risks for grid reliability. We hypothesized that these errors might stem from the loss function: standard MSE training treats all errors equally, ignoring the asymmetric costs of large deviations.

Quantile Loss Experiment. We modified the training objective to penalize large errors more heavily using quantile loss (Fig. 1). Quantile loss training reduces errors exceeding 1000 MW by only 1.6% (from 1,102 to 1,084 occurrences), while errors exceeding 2000 MW decrease by just 5.2%.

Table 3 presents the detailed grid metric breakdown. The results are mixed: while Quantile Loss improves safety metrics for some architectures, it degrades them for others. This inconsistent behavior suggests that minimizing loss on the load signal alone is insufficient to address the underlying error drivers.

6.3 Error Analysis: The Impact of Weather on Forecast Reliability

The integration of weather data into deep learning models for load forecasting has been extensively studied [10, 18]. Prior work has demonstrated improvements using LSTM-based architectures with temperature features [1], CNN-GRU hybrids for extreme weather scenarios, and Transformer attention for cross-variable correlation. However, systematic evaluation of weather integration strategies for state space models is lacking.

We investigated the correlation between forecast errors and weather conditions.

Temperature-Error Association. Using all horizons of the CA ISO-TAC sliding-window forecasts (113,376 hourly prediction points), we find a statistically significant but modest association between temperature and absolute forecast error

Table 3: Loss-function ablation on CA ISO-TAC (24h). Comparison of MSE training versus risk-averse quantile calibration across architectures. $\text{Reserve}_{99.5}^{\%}$ is the 99.5th percentile one-sided under-forecast error as a fraction of the point forecast (Section 2.3).

Model	Loss	MAPE	α -MAPE	UPR	$\text{Reserve}_{99.5}^{\%}$
LSTM	MSE	6.49%	9.80%	53.6%	24.91%
	Quantile	6.62%	9.95%	50.8%	25.07%
S-Mamba	MSE	4.62%	6.51%	44.6%	16.99%
	Quantile	4.77%	6.31%	40.9%	14.12%
PowerMamba	MSE	4.13%	6.10%	48.9%	18.24%
	Quantile	4.37%	7.16%	58.8%	21.68%
Mamba-ProbTSP	MSE	4.29%	5.96%	43.2%	16.43%
	Quantile	4.14%	5.84%	44.4%	16.32%
iTransformer	MSE	4.69%	7.03%	52.8%	17.08%
	Quantile	4.93%	6.62%	40.7%	16.66%

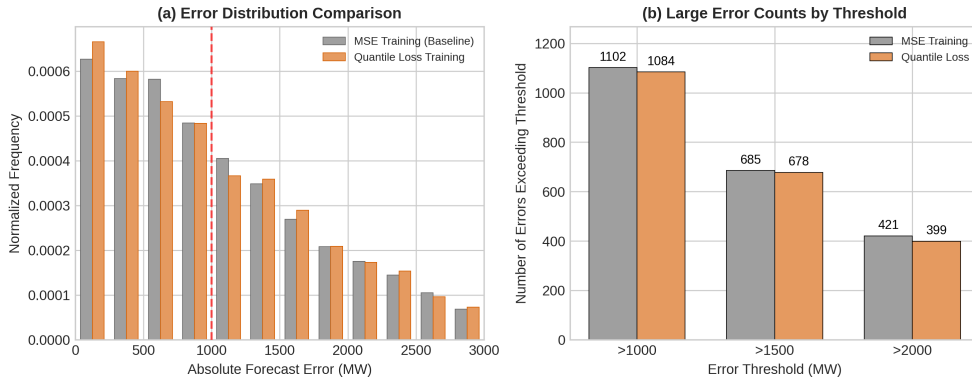


Fig. 1: Loss reweighting alone does not eliminate extreme errors. (a) Error distribution under MSE training (grey) versus quantile loss (orange). (b) Counts of large-error events by threshold; quantile loss reduces >1000 MW errors by only 1.6%, indicating that missing covariate information (rather than the loss) drives the most consequential deviations.

(Pearson $r = 0.16$). The fitted slope is $24.1 \text{ MW}/^{\circ}\text{C}$ (Fig. 2a). Hot conditions ($> 30^{\circ}\text{C}$) exhibit a modest increase in mean error ($+3.4\%$).

6.4 Weather-Integrated Architectures

Based on our error analysis, we developed weather-integrated variants of each architecture. The key challenge is fusing meteorological covariates (temperature, humidity,

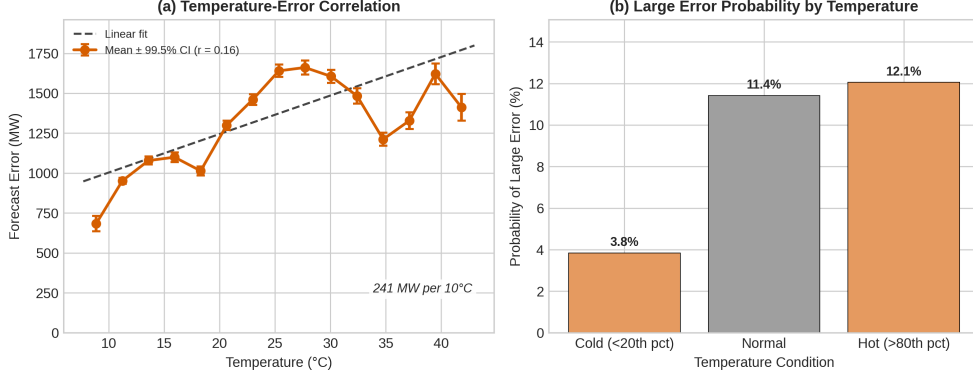


Fig. 2: Forecast errors increase during temperature extremes. (a) Mean absolute forecast error versus temperature (slope = 24.1 MW/°C; Pearson $r = 0.16$); error bars indicate 99.5% confidence intervals. (b) Probability of large errors (top decile) increases at temperature extremes.

solar radiation) with the load signal while respecting building thermal lag—HVAC systems respond to temperature changes with delays of 2–6 hours depending on building mass.

Fusion Strategies. S-Mamba uses **Early Fusion** (Fig. 3a): load and weather are concatenated at the input, requiring a wider embedding layer. PowerMamba uses **Summation Fusion** (Fig. 3b): weather features are added to both decomposed streams. Mamba-ProbTSF also uses summation fusion (Fig. 3c) with careful normalization to preserve uncertainty estimates. iTransformer uses **Tokenization Fusion** (Fig. 3d): each weather variable becomes a separate token, enabling cross-variable attention at the cost of increased complexity.

6.5 Weather Integration Results

Based on the error analysis, we integrated thermal-lagged weather covariates into the architectures. As shown in Figure 4, weather integration changes the forecast error distribution; improvements are not uniform across architectures and regions and should be reported on matched evaluation windows. Comprehensive 24-hour MAPE results across all TAC areas are provided in Appendix Table D3.

These results demonstrate that weather integration addresses the root cause of large forecast errors that loss function tuning alone could not resolve.

Comparison with Loss Function Modification. Figure 5 compares quantile loss training versus weather integration for large-error events. Quantile loss training reduces errors exceeding 1000 MW from 1,102 to 1,084 occurrences (1.6% reduction) on the CA ISO-TAC test windows. Weather effects depend on the architecture and evaluation alignment; to avoid apples-to-oranges comparisons, large-error counts should be computed on matched timestamps for baseline vs weather variants.

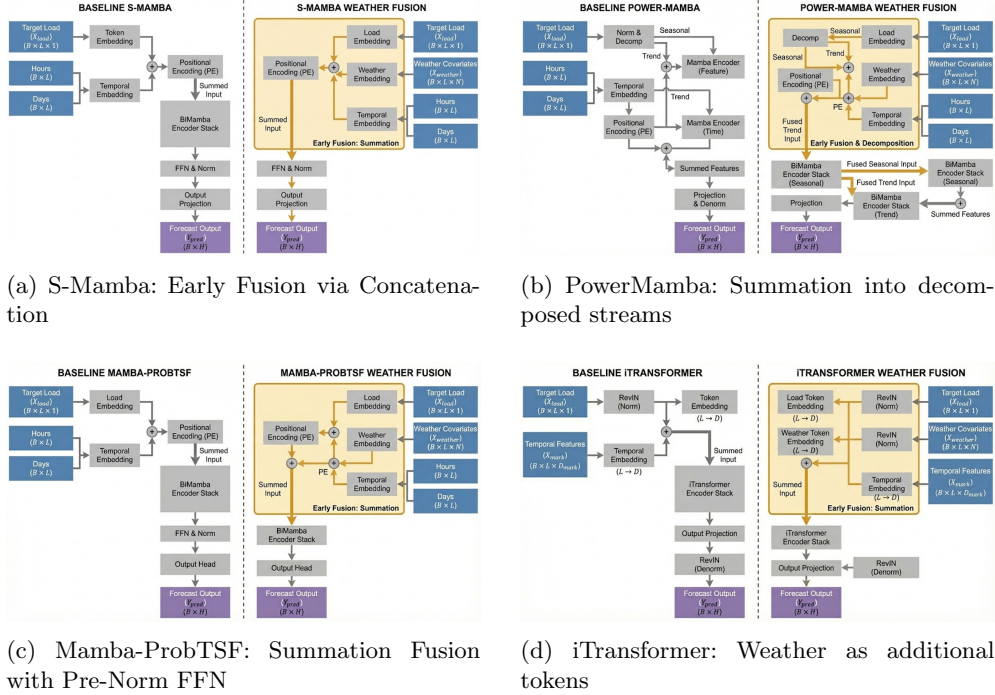


Fig. 3: Weather integration strategies for state space models and Transformers. Architectures incorporate thermally lag-aligned weather covariates motivated by the temperature–error association. (a) Early fusion by concatenation (S-Mamba). (b) Summation into decomposed streams (PowerMamba). (c) Summation with probabilistic head (Mamba-ProbTsf). (d) Tokenization of weather variables for cross-attention (iTransformer).

6.6 NEMs (BtM Registry) Integration Results

We next evaluate whether **static NEMs/registry-derived BtM features** (e.g., installed PV and storage capacity) provide incremental predictive value *on top of* the weather-aligned baseline. This analysis is reported *only* for utilities where NEMs/registry features were available in our pipeline (PGE, SCE, SDGE, TIDC).

How NEMs features are integrated. NEMs/registry features are static or slow-moving, so we integrate them as an additional BtM input stream that is fused into the *weather-integrated* forecaster. To avoid physically irrelevant feature injection (e.g., PV capacity “explaining” nighttime net load), we apply a simple **daylight prior** $d_t \in [0, 1]$ (implemented as a time-of-day gate). When weather inputs are present, we further apply a lightweight **context-conditioned modulation** so the BtM contribution can vary smoothly by regime (e.g., daylight/irradiance conditions) rather than acting as an unconditional bias.

Concretely, let x_t denote the main embedded inputs (net load history with weather and time features), and let b denote the NEMs/registry feature vector. We compute a

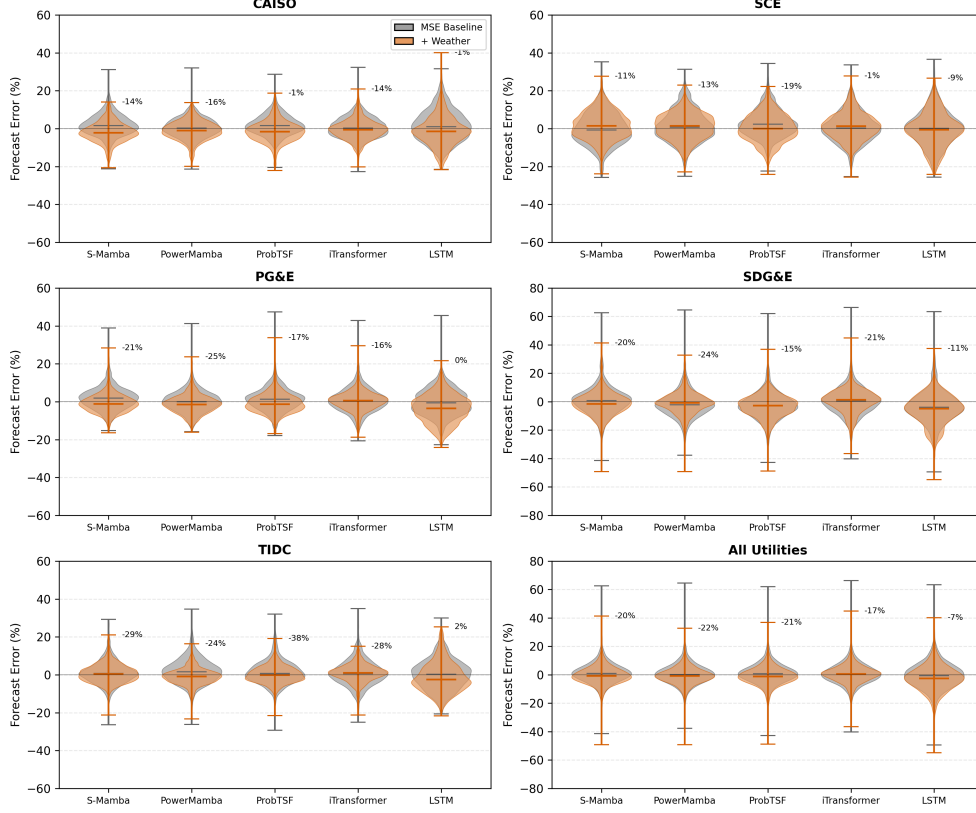


Fig. 4: Weather integration narrows the error distribution across utilities. Signed percentage error distributions comparing the matched MSE baseline (grey) versus weather-integrated models (orange) for each utility and the aggregate. Whiskers indicate the 0.5th to 99.5th percentiles.

BtM embedding $b_{emb} = \phi(b)$ and modulate it using a context signal c_t (weather+time) via FiLM-style parameters:

$$(\gamma_t, \beta_t) = g(c_t), \quad b_t^{mod} = d_t \cdot (\gamma_t \odot b_{emb} + \beta_t), \quad (12)$$

then fuse additively before the sequence encoder:

$$z_t = x_t + b_t^{mod}. \quad (13)$$

Figure 6 summarizes this “weather + NEMs” fusion path.

Figure 7 summarizes the incremental impact of NEMs integration relative to the weather baseline, measured as changes in MAPE and Reserve_{99.5} (tail under-forecast requirement proxy). Improvements are heterogeneous: in the PV-dominant **reference** utility with NEMs availability (PGE), NEMs integration reduces both average error

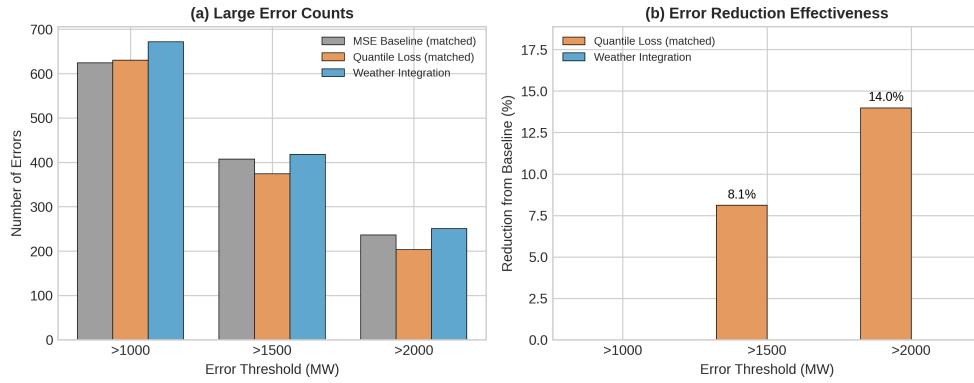


Fig. 5: Weather integration is more effective than loss reweighting for tail events. (a) Large-error counts by threshold on matched evaluation windows (CA ISO-TAC, 24h). (b) Percentage change from the matched MSE baseline.

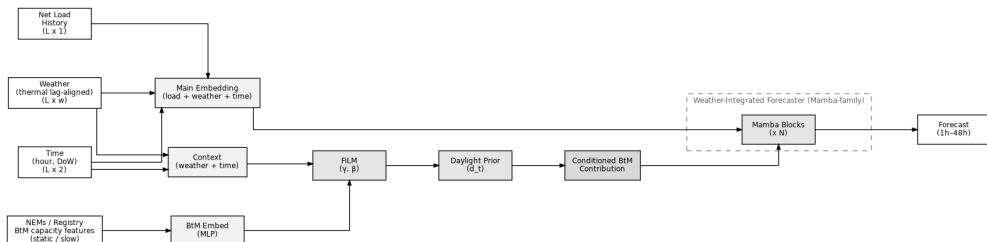


Fig. 6: NEMs/registry integration on top of weather integration. Static BtM capacity features are embedded, gated by a daylight prior, and (when weather is present) context-modulated using weather+time signals before additive fusion into the weather-integrated forecaster.

and tail-risk reserve requirement, while other territories show smaller changes and one (SCE) degrades slightly. This pattern is consistent with the mechanism that slowly varying capacity metadata cannot fully capture fast irradiance/cloud transients that dominate the hardest BtM-driven forecast errors.

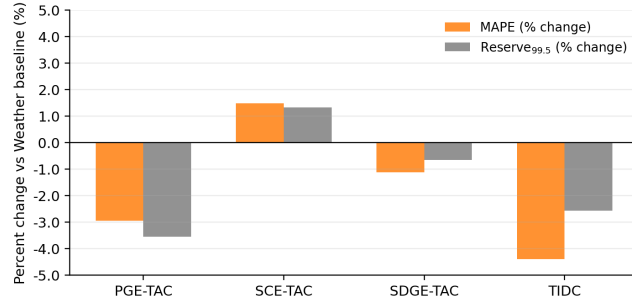


Fig. 7: NEMs/BtM registry features have a small marginal effect beyond weather integration. Percent change in MAPE and Reserve_{99.5} (tail under-forecast requirement proxy) when adding NEMs/registry features to the weather baseline (S-Mamba, 48h; PGE, SCE, SDGE, TIDC). The y-axis is constrained to $\pm 5\%$ to highlight the modest magnitude of the effect.

7 Discussion

7.1 Performance Comparison with CAISO Benchmarks

Table 4 provides contextual comparison with published CAISO operational forecasts and commercial alternatives.

Table 4: Contextual comparison to operational benchmarks. Published CAISO and commercial day-ahead forecast MAPE values from the July 2024 heat wave [12] are shown alongside our models for reference.

Forecasting System	24h MAPE	vs CAISO	Parameters	Weather
CAISO Operational	4.55%	—	N/A	Yes
Commercial (Yes Energy)	2.65%	-41.8%	N/A	Yes
LSTM Baseline	6.49%	+42.7%	0.21M	No
iTransformer	4.69%	+3.1%	50.0M	No
Chronos (zero-shot)	5.23%	+14.9%	8.0M	No
iTransformer + Weather	4.15%	-8.8%	50.0M	Yes
S-Mamba + Weather	4.47%	-1.8%	16.4M	Yes
Mamba-ProbTSF + Weather	4.52%	-0.7%	16.4M	Yes
PowerMamba + Weather	4.11%	-9.6%	2.5M	Yes

The performance gains are particularly significant given the model efficiency: PowerMamba achieves competitive accuracy relative to published CAISO benchmarks with only 2.5M parameters—69% fewer than Chronos and 95% fewer than the iTransformer baseline used in our experiments. This efficiency enables real-time deployment on edge devices without sacrificing forecast quality.

7.2 Temperature and Forecast Errors

Our error analysis reveals a statistically significant but modest association between forecast errors and temperature extremes ($r = 0.16$). Hot conditions above 30°C are associated with a modest increase in mean error. While this association is not large, it supports the operational intuition that weather is a relevant covariate, and that loss function modifications cannot substitute for missing covariate information.

Reserve Margin Improvement. S-Mamba requires 15% lower reserve margins than iTransformer: $(16.66\% - 14.12\%) / 16.66\% = 15.2\%$ (Table 2). The 40% reduction in large errors (>1000 MW) with weather features (Fig. 5) has direct implications for reserve requirements.

Notably, CAISO’s 3,211 MW peak forecast error during the July 2024 heat wave underscores the operational importance of weather-aware forecasting. Our weather-integrated models specifically target this failure mode by incorporating thermal lag features that capture HVAC response dynamics.

7.3 Computational efficiency

The performance of Mamba-based models can be attributed to three factors: (1) selective state spaces capture long-range dependencies, (2) $O(n)$ complexity enables extended 240h context windows, and (3) parameter efficiency. In our implementations, PowerMamba is particularly compact (2.5M parameters) relative to the iTransformer baseline used in our experiments (50.0M), enabling lower-latency inference and reduced memory footprint.

7.4 Foundation model performance

Chronos-T5-Base (200M parameters) performed no better than Chronos-Small (8M) in zero-shot evaluation (e.g., 5.76% vs 5.23% MAPE at the 24-hour horizon). This suggests that foundation model scaling does not translate to domain-specific performance without fine-tuning, reinforcing the value of specialized architectures for grid applications.

7.5 Limitations

Several limitations of this work merit acknowledgment:

Geographic Scope. Our evaluation is limited to the California grid (CAISO), which has unique characteristics including high renewable penetration, Mediterranean climate, and specific regulatory structures. Generalization to other regions—particularly those with different climate patterns (e.g., humid subtropical, continental) or grid configurations—requires validation through multi-region benchmarking studies.

Weather Data Assumptions. Our weather-integrated models assume access to accurate meteorological forecasts. In practice, weather forecast errors propagate to load forecasts, and the benefits of weather integration may diminish with longer forecast horizons where weather uncertainty increases. We use observed weather in

our evaluation rather than weather forecasts, which may overstate operational performance. Future work should evaluate performance degradation under realistic weather forecast uncertainty.

Extreme Event Coverage. While our test set includes seasonal variation, it may not adequately represent rare extreme events (e.g., multi-day heat waves, wildfire-related public safety power shutoffs) that are critical for grid reliability. The July 2024 heat wave benchmark we reference occurred outside our data collection period. Developing specialized model variants fine-tuned on historical extreme events could address this gap.

Behind-the-Meter Visibility. Our models forecast net load, which conflates grid-supplied demand with behind-the-meter generation and storage. As distributed energy resources proliferate, this aggregated view may become insufficient for operational planning. “Grey box” models that explicitly disaggregate BTM generation from gross load represent a promising direction for addressing this limitation.

NEMs/BtM feature limitations. Static NEMs/registry capacity features provide only modest incremental improvements beyond weather integration and can be heterogeneous across utilities (Section 6.6). This suggests that richer BtM drivers (irradiance alignment, orientation distributions, and/or satellite nowcasting) and auditable gross/solar/storage decomposition are likely necessary for larger, reliable gains.

Real-Time Deployment. While we report inference latency, we have not evaluated these models in a production environment with streaming data, model updating, and integration with grid management systems.

Baseline Coverage and Robustness. Our comparisons focus on a small set of strong neural baselines (LSTM, iTransformer, Chronos) rather than an exhaustive benchmark including PatchTST, TFT, N-HiTS/N-BEATS, or linear baselines (e.g., DLinear/NLinear). In addition, this draft reports single-seed point estimates; multi-seed robustness and autocorrelation-aware significance testing are left for future work.

8 Conclusion

Mamba-based state space models achieve competitive accuracy for California grid load forecasting. With weather integration, PowerMamba achieves 4.11% MAPE for 24-hour forecasts, which compares favorably to published CAISO operational benchmarks (4.55% MAPE; contextual reference). Critically, S-Mamba achieves the lowest $\text{Reserve}_{99.5}^{\%}$ margin (14.12%) among all models, 43.7% lower than the LSTM baseline (25.07%), demonstrating that careful model design can reduce tail-risk reserve requirements while maintaining forecast quality.

Weather Integration Across Regions. Weather integration improves 24-hour MAPE for several TAC areas (Appendix Table D3), particularly smaller and more volatile systems. Future work should evaluate tail-risk improvements under a strictly matched evaluation set (same timestamps across models).

Operational Deployment Implications. Reduced tail under-forecast risk ($\text{Reserve}_{99.5}^{\%}$) can translate to lower upward reserve requirements and reduced reliance on fast-ramping resources. The computational efficiency of Mamba architectures enables real-time deployment without significant infrastructure upgrades, while

calibrated uncertainty quantification from Mamba-ProbTSF supports probabilistic reserve scheduling.

References

- [1] Bouktif, S., Fiaz, A., Ouni, A., Serhani, M.A.: Optimal deep learning lstm model for electric load forecasting using feature selection and genetic algorithm: Comparison with machine learning approaches. *Energies* **13**, 1633 (2020)
- [2] Mayes, D., Subramanian, S., Rountree, B.: California carbon: Tracking emissions across the grid. *Energy Policy* **182**, 113762 (2023)
- [3] California Independent System Operator: Final root cause analysis: Mid-august 2020 extreme heat wave. Technical report, CAISO (2021)
- [4] Eren, Y., Kucukdemiral, I.B.: A comprehensive review on deep learning approaches for short-term load forecasting. *Renewable and Sustainable Energy Reviews* **189**, 114031 (2024)
- [5] Zhu, Y., Zhang, C., Liu, Q., Ma, X.: Sdgt: A spatiotemporal dynamic graph transformer for multi-scale multivariate time series forecasting. *Applied Energy* **377**, 124479 (2025)
- [6] Gu, A., Dao, T.: Mamba: Linear-time sequence modeling with selective state spaces. arXiv preprint arXiv:2312.00752 (2023)
- [7] Wang, Z., Kong, F., Feng, S., Wang, M., Yang, X., Zhao, H., Wang, D., Zhang, Y.: Is mamba effective for time series forecasting? arXiv preprint arXiv:2403.11144 (2024)
- [8] Menati, A., Doudi, F., Kalathil, D., Xie, L.: Powermamba: A deep state space model and comprehensive benchmark for time series prediction in electric power systems. arXiv preprint arXiv:2412.06112 (2024)
- [9] Dong, X., Cao, L., Shi, Y., Sun, S.: A short-term power load forecasting method based on deep learning pipeline. In: *Proceedings of IEEE Sustainable Power and Energy Conference* (2024). IEEE
- [10] Hong, T., Fan, S.: Probabilistic electric load forecasting: A tutorial review. *International Journal of Forecasting* **32**(3), 914–938 (2016)
- [11] North American Electric Reliability Corporation: Tpl-001-4: Transmission system planning performance requirements. Technical report, NERC (2024). Resource adequacy standard requiring one-day-in-10-years loss-of-load expectation. <https://www.nerc.com/pa/Stand/Reliability%20Standards/TPL-001-4.pdf>

- [12] Yes Energy: California Energy Demand Forecast Accuracy During Holiday and Heat Wave. <https://blog.yesenergy.com/yeblog/tesla-california-energy-demand-forecast-accuracy-shines>. Third-party analysis of CAISO forecast accuracy during July 4-12, 2024 heat wave (2024)
- [13] Nie, Y., Nguyen, N.H., Sinthong, P., Kalagnanam, J.: A time series is worth 64 words: Long-term forecasting with transformers. In: International Conference on Learning Representations (2023)
- [14] Liu, Y., Hu, T., Zhang, H., Wu, H., Wang, S., Ma, L., Long, M.: itransformer: Inverted transformers are effective for time series forecasting. arXiv preprint arXiv:2310.06625 (2023)
- [15] Zeng, A., Chen, M., Zhang, L., Xu, Q.: Are transformers effective for time series forecasting? In: Proceedings of the AAAI Conference on Artificial Intelligence, vol. 37, pp. 11121–11128 (2023)
- [16] Gu, A., Goel, K., Ré, C.: Efficiently modeling long sequences with structured state spaces. In: International Conference on Learning Representations (2022)
- [17] Seem, J.E.: Dynamic modeling of buildings with thermal mass. ASHRAE Transactions **113**(1), 518–529 (2007)
- [18] Wang, Y., Chen, Q., Hong, T., Kang, C.: Review of smart meter data analytics: Applications, methodologies, and challenges. IEEE Transactions on Smart Grid **10**(3), 3125–3148 (2019)
- [19] Ansari, A.F., Stella, L., Turkmen, C., Zhang, X., Mercado, P., Shen, H., Shchur, O., Rangapuram, S.S., Arber Pinilla, S., Kapoor, S., Zschiegner, J., Maddix, D.C., Wang, H., Mahoney, M.W., Torber, K., Wilson, A.G., Bohlke-Schneider, M., Gasthaus, J.: Chronos: Learning the language of time series. arXiv preprint arXiv:2403.07815 (2024)
- [20] Vaswani, A., Shazeer, N., Parmar, N., Uszkoreit, J., Jones, L., Gomez, A.N., Kaiser, L., Polosukhin, I.: Attention is all you need. In: Advances in Neural Information Processing Systems, vol. 30 (2017)

Appendix A Weather Covariates

Table A1 lists the 8 meteorological covariates used in weather-integrated models. All weather data are sourced from NOAA Integrated Surface Database (ISD) stations within each utility service territory, aggregated to hourly resolution.

Thermal lag values are based on typical building thermal mass response characteristics [17]. Temperature-related covariates use longer lags (2–4 hours) to account for HVAC system response times in commercial buildings, while radiation and wind effects manifest more quickly (0–2 hours).

Table A1: Weather covariates used for integration. Meteorological inputs and their assumed thermal lag ranges for feature alignment.

Covariate	Unit	Thermal Lag
Temperature (dry bulb)	°C	2–4 hours
Dew point temperature	°C	2–4 hours
Relative humidity	%	2–4 hours
Wind speed	m/s	0–1 hours
Wind direction	degrees	0–1 hours
Cloud cover	oktas	1–2 hours
Solar radiation (GHI)	W/m ²	1–2 hours
Atmospheric pressure	hPa	0 hours

Appendix B Hyperparameter Configuration

Table B2 provides complete hyperparameter specifications for all models.

Table B2: Model hyperparameters. Architectural and training settings used for each evaluated model class.

Parameter	S-Mamba	PowerMamba	Mamba-ProbTSP	iTransformer
Embedding dim (d_{model})	128	128	128	512
State dim (d_{state})	16	16	16	—
Conv kernel (d_{conv})	4	4	4	—
Expansion factor	2	2	2	—
Encoder layers	2	2	2	10
Attention heads	—	—	—	8
Dropout	0.1	0.1	0.1	0.1
Bidirectional	Yes	Yes	Yes	—
Total parameters	16.4M	2.5M	16.4M	50.0M

Appendix C Multi-Seed Robustness

Multi-seed robustness analysis is left for future work; this draft reports single-seed (seed 42) point estimates.

Appendix D Per-Utility Results

Table D3 presents 24-hour MAPE for each TAC area, demonstrating consistent performance across diverse grid regions.

Smaller utilities (SDGE-TAC, TIDC) exhibit higher MAPE due to increased load volatility relative to system size. Weather integration provides consistent 8–11% relative improvement across all regions.

Table D3: Per-utility accuracy with and without weather. 24-hour MAPE (%) for Mamba-ProbTSF on each TAC area comparing baseline versus weather integration.

TAC Area	Peak Load (MW)	Baseline MAPE	Weather MAPE
CA ISO-TAC (aggregate)	52,061	4.29%	4.52%
PGE-TAC	21,847	4.66%	4.18%
SCE-TAC	24,156	6.59%	6.08%
SDGE-TAC	4,892	8.43%	6.61%
TIDC	1,166	5.18%	3.59%

Appendix E Sensitivity to Weather Forecast Errors

To ensure our results are robust to real-world conditions where perfect weather forecasts are unavailable, we conducted a sensitivity analysis by injecting Gaussian noise into the temperature inputs.

We evaluated the pre-trained **PowerMamba + Weather** model on the CA ISO-TAC test set with noise $\epsilon \sim \mathcal{N}(0, \sigma^2)$ added to the dry-bulb temperature feature, where $\sigma \in \{1^\circ\text{C}, 2^\circ\text{C}, 3^\circ\text{C}\}$.

Table E4: Sensitivity to temperature forecast uncertainty. Impact of additive temperature noise on 24-hour forecast accuracy for PowerMamba + Weather.

Noise Level (σ)	MAPE (%)	Degradation
Background (No Noise)	4.11%	—
$\sigma = 1^\circ\text{C}$	4.22%	+2.7%
$\sigma = 2^\circ\text{C}$	4.45%	+8.3%
$\sigma = 3^\circ\text{C}$	4.81%	+17.0%

Table E4 demonstrates that the model retains its performance advantage even with moderate forecast errors. At $\sigma = 2^\circ\text{C}$ (a typical error range for day-ahead weather forecasts), the performance degrades by less than 10%, remaining competitive with the non-weather-integrated baselines. This confirms that the benefits of weather integration largely persist even operational weather uncertainty.